NASA Technical Memorandum 81473

SIMILARITY TESTS OF TURBINE VANES - EFFECTS OF CERAMIC THERMAL BARRIER COATINGS

(NASA-TM-81473) SIMILARITY TESTS OF TURBINE VANES, EFFECTS OF CERAMIC THERMAL BARRIER COATINGS (NASA) 14 p HC A02/MF A01 CSCL 20D

N80-21706

Unclas
G3/34 46821

Herbert J. Gladden
Lewis Research Center
Cleveland, Ohio

Prepared for the
1980 National Heat Transfer Conference
sponsored by the Heat Transfer and Gas Turbine Divisions
of the American Society of Mechanical Engineers
Orlando, Florida, July 27-30, 1980

NOMENCLATURE

A	heat transfer area
C_1	constant
h	heat transfer coefficient
k	thermal conductivity
Nu	Nusselt number
P	pressure
Pr	Prandtl number
q	heat flux
R	gas constant
Re	Reynolds number
T	temperature
w	mass flow rate
x	surface distance
Γ	function of specific heat ratios
γ	specific heat ratio
μ	viscosity
τ	wall or coating thickness; characteristic dimension
φ	$(T_g - T_{wo})/(T_g - T_{ci})$

SUBSCRIPTS:

c	coolant
ci	coolant inlet
e	engine
g	gas inlet
ge	effective gas
t	test
u	uncoated condition
w	wall
wi	coolant side of metal wall
wo	gas side of metal wall
zi	metal-ceramic interface
zo	gas side of ceramic
z	ceramic

SUPERSCRIPTS:

(e)	engine conditions
(t)	test conditions
-	average

INTRODUCTION

Ceramic thermal barrier coatings are being considered for the hot section components of gas turbine engines to supplement the thermal protection provided by various air-cooling schemes. The thermal performance of these coated components are often evaluated at reduced gas/coolant temperatures and pressures to avoid the complexity and expense of testing at actual engine gas/coolant conditions. However, extrapolation (scaling) of these test results to engine conditions can lead to erroneous conclusions unless the thermal effects of variations in ceramic, metal, gas, and coolant thermal conductivities are considered.

Several techniques exist which can be used to establish the reduced gas/coolant temperatures and pressures (Refs. (1) to (4)) necessary for testing turbine components at similarity conditions. The approach used in each of these references is somewhat different but the results and conclusions are basically the same. That is, kinetic, dynamic, and thermal similarity of the gas and coolant can be maintained between test conditions and engine conditions by maintaining an equality of various dimensionless parameters such as Reynolds, Prandtl, and Mach numbers. References (2) and (3) also discuss the need to maintain similarity of the material thermal conductivity to achieve a similar thermal performance of the hardware at both test and engine conditions. Reference (3), however, concludes that the thermal conductivity effect is not significant for the conditions and material considered. Reference (4), however, shows that gas, coolant, and metal thermal conductivity variations between test and engine conditions leads to a 4.0 to 4.5 percent error in the cooling effectiveness parameter φ used for comparison. Reference (5) investigated cases of a ceramic thermal barrier coating material added to turbine vane airfoil and found that the addition of the ceramic could result in errors when data comparisons are made between ceramic coated and uncoated turbine vanes and when these data are extrapolated to engine conditions. A correction technique developed in reference (5) resulted in correction factors which were of opposite sign between the uncoated vane data and the coated vane data.

The analysis of reference (5) is used herein to predict the data corrections required for ceramic coated and uncoated turbine vanes tested at reduced gas/coolant temperatures and pressures. These corrected data are then compared to actual data taken at engine conditions. The results are also presented as an error between engine and test conditions for turbine vane cooling effectiveness parameters from 0.3 to 0.6.

APPARATUS AND EXPERIMENTAL PROCEDURE

Cascade Facility

The cascade facility was designed for continuous operation at gas temperatures and pressures up to 1600 K and 100 N/cm^2 (absolute). A schematic of the cascade facility is shown in Fig. 1(a). The cascade facility consisted of five major components shown in Fig. 1(b): an inlet section, a high temperature combustor section, a circular-to-annular transition section, the test section, and an exit section. The transition, test, and exit section were water-cooled to achieve structural durability during high-temperature operation. A more detailed description is contained in reference (6).

The high temperature combustor section was removed and replaced by a spool piece for low-temperature tests in the facility. Hot combustion air was then supplied to the test section by the low temperature combustor shown in Fig. 1(a). The low temperature combustor was capable of supplying combustion air to the test section at temperatures up to 900 K.

The test section was a 23° annular sector of a vane row and contained four vanes and five flow channels. A plan view of the test section, showing the test vane (vane number 2) and selected instrumentation, is presented in Fig. 2. The slave vanes complete the flow channels for the test vane and serve as radiation shields between the test vane and the water-cooled walls of the test section. The test section walls were coated with yttria stabilized zirconia to increase the surface temperature and minimize net thermal radiation from the test vane.

Vane

The turbine vane used in this investigation was a J-75 size airfoil with impingement cooling in the forward 2/3 of the airfoil and pin fin/film cooling in the aft 1/3 of the airfoil. A cross-sectional schematic of the airfoil and cooling configuration is shown in Fig. 3. The vane span was 9.78 cm and the midspan chord length was 6.28 cm. The wall thickness in the impingement cooled region was 0.152 cm. The vane airfoil shell material was MAR M-302.

The impingement insert had a staggered array of holes which were 0.051 cm in diameter. The spacing varied, depending on location, between 6.5 and 9 hole diameters span-wise and between 2.4 and 9 holes diameters chord-wise. The closely spaced holes were in the leading edge region (6.5 by 2.4) while the midchord region had larger spacings (9 by 9 on the pressure side and 8.5 by 8.5 on the suction side). The impingement hole- to heat-transfer-surface-spacing was approximately 1.5 hole diameters in the midchord region and approximately 2 hole diameters in the leading edge region. The impingement insert material was L-605.

There were 7 chord-wise rows of round pin fins in the split trailing edge. The three upstream rows had pin diameters of approximately 0.102 cm with a span-wise spacing of 0.406 cm and a chord-wise spacing of 0.353 cm. The last four rows had pin diameters of 0.076 cm with a span-wise spacing of 0.305 cm and a chord-wise spacing of 0.264 cm. The width of the split trailing edge channel at the point of discharge was 0.089 cm.

A single row of film cooling holes was located between pin fin rows 3 and 4 on the vane pressure surface and ejected air at an angle of 30° to the vane surface in the span-wise direction. The purpose of these holes was to provide a sufficient flow area to accommodate the design coolant flow requirements.

Thermal Barrier Coating

The procedure used for depositing ceramic coating (Ref. (7)) onto the vane metal substrate was to prepare the substrate surface by grit-blasting, plasma-spray on a bond coat of NiCrAly, and then plasma-spray on the ceramic coating of yttria stabilized zirconia. The measured surface roughness of the applied ceramic coating was 8 to 10 micrometers, rms. However, the coating surface was polished with silicon carbide paper to a surface finish of about 3 micrometers, rms.

The bond and ceramic coatings were built up to the desired thickness by a succession of spray appli-

cations in the span-wise and chord-wise directions on the airfoil. The coatings were first applied to the vane leading edge, then to the trailing edge, and finally to the suction and pressure surfaces. The final total coating thickness was determined, after the polishing operation, by comparing 10X profiles of the airfoil before and after coating at each of the thermocouple locations. The ceramic coating thickness was then assumed to be the total thickness less the approximately 0.010 cm thick bond coat. The distribution of the coating thickness is given in Table I. The coating was tapered to negligible thickness at thermocouple location 12. This was necessary because of the film cooling holes aft of this location. The coating techniques were not sufficiently developed at the time to permit coating in the hole region without hole blockage.

Test Procedure

Thermal performance tests were made at the gas and coolant conditions given in Table II. The desired combustion gas temperature, pressure, and exit critical velocity ratio (0.85) were established and then the cooling-air flowrate was varied in a stepwise fashion from test point to test point. Steady state data were recorded at each of the cooling air and gas condition set-points. Ambient temperature cooling air was utilized for all test and engine conditions investigated. The data taken in the cascade at high gas temperatures and pressures are defined as engine data while the data taken at reduced gas temperatures and pressures are defined as test data.

INSTRUMENTATION

A radially traversing, sonic aspirated, type R (Platinum vs Platinum - 13% Rhodium) total temperature probe and a radially traversing total pressure probe provided the inlet gas conditions to the test vane (Fig. 2). The temperature distribution was measured upstream of channel 3 and the pressure distribution was measured upstream of channel 4. The inlet static pressure was measured only at the inner radius (hub) and was assumed to be constant across the gas stream. Static pressures were also measured at the exit midchannel position of channels 2, 3, and 4 at both the inner (hub) and outer (tip) radius platforms. These pressures were used to establish the midspan inlet and exit critical velocity ratios.

The midspan of the test vane airfoil was instrumented with an array of 12 Chromel-Alumel thermocouples. Figure 3 shows the relative location of these thermocouples with respect to the important features of the vane. Chord-wise thermocouple locations are given in Table I. The thermocouples were installed in slots EDM'ed in the exterior surface of the airfoil. The junction end of each thermocouple assembly was peened into the slot which effectively located the measuring station a specified distance from the bottom of the slot. The remainder of the slot over the thermocouple junction was filled by spot-welding a nickel-chromium material in the void and fairing the resultant construction to the original airfoil profile.

The construction of the thermocouple assemblies consisted of Chromel-Alumel thermoelements with magnesium oxide insulation in an Inconel-600 sheath. These assemblies were drawn to two sheath sizes, 0.05 and 0.025 cm outside diameter, with a closed-end grounded junction formed at one end. The three thermocouples near the leading edge were 0.025 cm diameter while the remaining thermocouples were of 0.05 cm diameter. A detailed description of the procedures utilized for thermocouple construction is given in reference (8). The slots for the 0.05 cm diameter thermocouples were 0.06 cm square while the slots for the 0.025 cm diameter thermocouples were 0.03 cm square. The measuring stations were nominally located 0.047 and 0.022 cm, respectively, below the gas side surface of the airfoil.

ANALYSIS METHOD

Similarity

References (2) and (3) show that Reynolds, Prandtl, and Mach numbers are sufficient to ensure dynamic, kinematic, and thermal similarity of the gas and coolant. Geometric similarity is maintained by using prototype engine component hardware. The following equations from references (2) and (3) establish the relationship between the engine and test conditions for similarity of both the hot gas and the coolant. These equations are based on an equality of momentum thickness Reynolds number and Mach number between the gas conditions of the engine and the similarity tests. In addition, an equality of the coolant Reynolds number is assumed.

$$\frac{P_g^{(t)}}{P_g^{(e)}} \frac{\mu_g^{(e)}}{\mu_g^{(t)}} \sqrt{\frac{(RT)_g^{(e)}}{(RT)_g^{(t)}} \frac{\Gamma_g^{(t)}}{\Gamma_g^{(e)}}} = 1 \qquad (1)$$

where

$$\Gamma_g = (\gamma)^{1/2} \left(\frac{2}{\gamma + 1}\right)^{(\gamma+1)/2(\gamma-1)} \qquad (2)$$

$$\left(\frac{w_c}{w_g}\right)^{(t)} = \left(\frac{w_c}{w_g}\right)^{(e)} \qquad (3)$$

$$\left(\frac{\mu_c}{\mu_g}\right)^{(t)} = \left(\frac{\mu_c}{\mu_g}\right)^{(e)} \qquad (4)$$

Maintaining similarity between engine and test conditions is necessary for duplicating thermal performance of the test components. The vane airfoil temperature distribution is generally sought by these tests of air-cooled turbine vanes. Reference (2) has shown that airfoil temperatures at engine conditions can be predicted from test results by a dimensionless temperature difference ratio. This ratio $(T_g - T_{wo})/(T_g - T_c)$, which is also called the cooling effectiveness φ, is based on a one-dimensional heat balance which assumes heat flow only from the gas to the coolant by convection and conduction.

Figure 4 is a representative cross-sectional schematic of a cooled turbine component with a layer of a ceramic coating on a metal substrate. The component temperature is assumed known at the metal-ceramic interface. The following one-dimensional equations can be written by neglecting lateral heat conduction in the component and radiation heat transfer between the component and the surrounding environment.

$$q_g = q_z = q_w = q_c \qquad (5)$$

where

$$q_g = h_g A_g (T_{ge} - T_{zo}) = Nu_g A_g (T_{ge} - T_{zo}) \frac{k_g}{\tau_g} \quad (6)$$

$$q_z = \frac{k_z A_z}{\tau_z} (T_{zo} - T_{zi}) \quad (7)$$

$$q_w = \frac{k_w A_w}{\tau_w} (T_{zi} - T_{wi}) = \frac{k_w A_w}{\tau_w} (T_{wo} - T_{wi}) \quad (8)$$

$$q_c = h_c A_c (T_{wi} - T_c) = Nu_c A_c (T_{wi} - T_c) \frac{k_c}{\tau_c} \quad (9)$$

T_{zi} is the metal-ceramic interface temperature which is also the gas side metal temperature T_{wo}. The inlet total gas and coolant temperature values can be substituted for local values (Ref. (9)) and the above equations then combined to obtain the following dimensionless form. It is also assumed that the heat transfer areas through the airfoil are equal (no curvature).

$$(T_g - T_{wo}) = \left(\frac{q\tau}{Nuk}\right)_g + \left(\frac{q\tau}{k}\right)_z \quad (10)$$

$$(T_{wo} - T_{ci}) = \left(\frac{q\tau}{k}\right)_w + \left(\frac{q\tau}{Nuk}\right)_c \quad (11)$$

$$\left(\frac{T_g - T_{wo}}{T_g - T_{ci}}\right) = \varphi_z = \left(\frac{1 + \frac{Nu_g k_g \tau_z}{k_z \tau_g}}{1 + \frac{Nu_g k_g \tau_c}{Nu_c k_c \tau_g} + \frac{Nu_g k_g \tau_w}{k_w \tau_g} + \frac{Nu_g k_g \tau_z}{k_z \tau_g}}\right) \quad (12)$$

A vane without the ceramic coating can be represented by equations (6), (8), and (9) where T_{zo} in equation (6) is replaced by T_{wo}.

$$\left(\frac{T_g - T_{wo}}{T_g - T_{ci}}\right) = \varphi_u = \left(1 + \frac{Nu_g k_g \tau_c}{Nu_c k_c \tau_g} \quad \frac{Nu_g k_g \tau_w}{k_w \tau_g}\right)^{-1} \quad (13)$$

In order that the model cooling effectiveness, φ, be directly applicable equations (12) and (13) show it is necessary to have Nusselt number similarity. Since heat transfer results follow the form $Nu = c_1 Re^m Pr^n$ Reynolds and Prandtl number similarity assures achieving the Nusselt number similarity required in equations (12) and (13). In addition, equality of the thermal conductivity ratios must be maintained if total similarity of the cooling effectiveness is to be maintained between test and engine conditions. This is, generally, not possible with most component materials.

Cooling Effectiveness Correction

The inability to maintain equality of the thermal conductivity ratios can lead to significant errors when using test data to predict component temperatures at engine conditions. The magnitude of this error can be determined by calculating the total derivative of equations (12) and (13) with respect to these variables.

$$d\varphi = \frac{\partial\varphi}{\partial\left(\frac{k_g}{k_z}\right)} d\left(\frac{k_g}{k_z}\right) + \frac{\partial\varphi}{\partial\left(\frac{k_g}{k_w}\right)} d\left(\frac{k_g}{k_w}\right) + \frac{\partial\varphi}{\partial\left(\frac{k_g}{k_c}\right)} d\left(\frac{k_g}{k_c}\right) \quad (14)$$

Reference (4) has shown that, since the ratio h_g/h_c is proportional to k_g/k_c, correcting for the gas-to-coolant thermal conductivity ratio between test and engine conditions is equivalent to correcting the heat transfer coefficient in a simplified model. The error model represented by equation (14) can also be used to calculate a correction factor between test data and engine data.

The first partial derivative in equation (14) becomes

$$\frac{\partial\varphi_z}{\partial\left(\frac{k_g}{k_z}\right)} = \frac{\left(\frac{Nu_g}{Nu_c}\frac{\tau_c}{\tau_g}\frac{k_g}{k_c} + Nu_g\frac{\tau_w}{\tau_g}\frac{k_g}{k_w}\right) Nu_g \frac{\tau_z}{\tau_g}}{\left(1 + \frac{Nu_g}{Nu_c}\frac{\tau_c}{\tau_g}\frac{k_g}{k_c} + Nu_g\frac{\tau_w}{\tau_g}\frac{k_g}{k_w} + Nu_g\frac{\tau_z}{\tau_g}\frac{k_g}{k_z}\right)^2} \quad (15)$$

The second partial derivative in equation (14) becomes

$$\frac{\partial\varphi_z}{\partial\left(\frac{k_g}{k_w}\right)} = -\frac{\left(1 + Nu_g\frac{\tau_z}{\tau_g}\frac{k_g}{k_z}\right) Nu_g \frac{\tau_w}{\tau_g}}{\left(1 + \frac{Nu_g}{Nu_c}\frac{\tau_c}{\tau_g}\frac{k_g}{k_c} + Nu_g\frac{\tau_w}{\tau_g}\frac{k_g}{k_w} + Nu_g\frac{\tau_z}{\tau_g}\frac{k_g}{k_z}\right)^2} \quad (16)$$

The third partial derivative in equation (14) becomes

$$\frac{\partial\varphi_z}{\partial\left(\frac{k_g}{k_c}\right)} = -\frac{\left(1 + Nu_g\frac{k_g}{k_z}\frac{\tau_z}{\tau_g}\right)\frac{Nu_g}{Nu_c}\frac{\tau_c}{\tau_g}}{\left(1 + \frac{Nu_g}{Nu_c}\frac{\tau_c}{\tau_g}\frac{k_g}{k_c} + Nu_g\frac{\tau_w}{\tau_g}\frac{k_g}{k_w} + Nu_g\frac{\tau_z}{\tau_g}\frac{k_g}{k_z}\right)^2} \quad (17)$$

Finally, combining equations (15) to (17) and simplifying, the correction factor for a ceramic coated turbine vane is

$$\Delta\varphi_{z,e-t} = \varphi^2_{z,t}\left[\left(\frac{1-\varphi}{\varphi}\right)_{z,t}\left(Nu_g\frac{\tau_z}{\tau_g}\right)_t \Delta\left(\frac{k_g}{k_z}\right)_{e-t} - \left(Nu_g\frac{\tau_w}{\tau_g}\right)_t \Delta\left(\frac{k_g}{k_w}\right)_{e-t} - \left(\frac{Nu_g}{Nu_c}\frac{\tau_c}{\tau_g}\right)_t \Delta\left(\frac{k_g}{k_c}\right)_{e-t}\right] \Bigg/ \left[\left(1 + Nu_g\frac{\tau_z}{\tau_g}\frac{k_g}{k_z}\right)_t\right] \quad (18)$$

where

$$\Delta\left(\frac{k_g}{k_z}\right)_{e-t} = \left(\frac{k_g}{k_z}\right)_e - \left(\frac{k_g}{k_z}\right)_t$$

$$\Delta\left(\frac{k_g}{k_w}\right)_{e-t} = \left(\frac{k_g}{k_w}\right)_e - \left(\frac{k_g}{k_w}\right)_t$$

and

$$\Delta\left(\frac{k_g}{k_c}\right)_{e-t} = \left(\frac{k_g}{k_c}\right)_e - \left(\frac{k_g}{k_c}\right)_t$$

The correction factor for an uncoated turbine vane is written as follows

$$\Delta\varphi_{u,e-t} = -\varphi^2_{u,t}\left[\left(Nu_g \frac{\tau_w}{\tau_g}\right)_t \Delta\left(\frac{k_g}{k_w}\right)_{e-t} + \left(\frac{Nu_g}{Nu_c}\frac{\tau_c}{\tau_g}\right)_t \Delta\left(\frac{k_g}{k_c}\right)_{e-t}\right] \quad (19)$$

Finally, the cooling effectiveness at engine conditions can be defined as the cooling effectiveness at test conditions plus the correction factor.

$$\varphi_e = \varphi_t + \Delta\varphi_{e-t} \quad (20)$$

All the terms in these equations for the correction factors are known or can be calculated. The gas side heat transfer coefficient can be calculated by whatever method the user has most confidence in modeling his experiment. The turbulent flat plat correlation is used herein.

$$h_g = 0.029\left(\frac{k_g}{x}\right) Re^{0.8} Pr^{1/3} \quad (21)$$

The gas and coolant thermodynamic and transport properties are taken from reference (10) while the metal and ceramic thermal conductivity values are taken from references (11) and (12), respectively.

RESULTS AND DISCUSSION

The similarity relationship of turbine inlet gas temperature and pressure expressed by equation (1) is shown in Fig. 5. One point on each curve represents a typical gas turbine engine with a turbine inlet temperature and pressure of 1550 K and 8.3 atm for the uncoated vane and 1440 K and 8.6 atm for the ceramic coated vane. The inlet coolant temperature assumed for these engine conditions was 300 K (see Table II). Choosing either a test gas temperature or pressure fixes the other, and also fixes all other parameters which satisfy the similarity relationships. The reduced gas temperature and pressure test conditions were 890 K and 4.5 atm for the uncoated vane and 920 K and 5.2 atm for the coated vane. The test condition coolant temperature was ambient air at 300 K which was not the 180 K required by similarity constraints. The discussion that follows will refer to data taken at high gas temperature and pressure as "engine data" and will refer to data taken at reduced gas temperature and pressure as "test data."

Cooling effectiveness correction factors were calculated by the procedure discussed in the ANALYSIS METHOD section and the test and engine conditions selected for study. Since the coolant inlet temperature for the test data was greater than that required for similarity a correction procedure similar to that developed in reference (4) was used to determine its effect on the cooling effectiveness. This correction factor is combined with the corrections for the ceramic and metal thermal conductivity effects. These net total correction factors are shown in Fig. 6 as a percent correction versus the cooling effectiveness. The net correction for the ceramic coated vane, at the conditions investigated, is essentially zero near a φ of 0.4 and minus 3 percent at a φ of 0.57. An analysis of the various terms of the correction equation show that a positive correction for the ceramic is off-set by negative corrections for both the metal and the coolant thereby reducing the net effect to nearly zero. In constrast, the net correction for the uncoated vane is strictly negative, composed only of the metal and the coolant correction factor terms, and is a function of the cooling effectiveness. The correction factor term for the coolant was about the same for both the coated and uncoated vane.

The effects of these correction factors, when applied to the average cooling effectiveness test data of the uncoated vane, are shown in Fig. 7. The average cooling effectiveness was based on the area weighted average airfoil temperature and the inlet gas and coolant temperatures. The uncorrected test data are shown to be considerable higher than the engine data. However, corrected test data (using correction factors in Fig. 6) are shown to compare quite well with the engine data.

The correction factors for the ceramic coated vane test data were nearly zero at cooling effectiveness values of about 0.4 and decreased to minus 3 percent at a cooling effectiveness of about 0.57. A comparison of corrected test and engine cooling effectiveness data in Fig. 8 shows good agreement.

The importance of correcting the test data is shown in Fig. 9 which is a cross-plot of Figs. 7 and 8. A comparison of the uncorrected test data of ceramic coated and uncoated turbine vanes would erroneously show the thermal barrier coating to be ineffective. A comparison of test data corrected for thermal conductivity and engine data of ceramic coated and uncoated vanes show that the coating actually increases the cooling effectiveness by an average of about 12.5 percent.

CONCLUSIONS

The thermal performance of a turbine vane can be evaluated reliably at reduced gas and coolant conditions. However, thermal conductivity corrections are required for the data at reduced conditions. These corrections for a ceramic thermal barrier coated vane are significantly different than the corrections for an uncoated vane. Comparison of uncorrected test data, therefore, would show erroneously that the thermal barrier coating was ineffective. When thermal conductivity corrections are applied to the test data these data are then shown to be representative of engine data and also show that the thermal barrier coating increases the vane cooling effectiveness by an average of 12.5 percent.

REFERENCES

1 Sucec, J., "Application of Differential Similarity to Finding Nondimensional Groups Important in Tests of Cooled Engine Components," NASA TM X-3484, 1977.

2 Gladden, H. J. and Livingood, J. N. B., "Procedure for Scaling of Experimental Turbine Vane Airfoil Temperatures from Low to High Gas Temperature," NASA TN D-6510, 1971.

3 Colladay, R. S. and Stepka, F. S., "Similarity Constraints in Testing of Cooled Engine Parts," NASA TN D-7707, 1974.

4 Kinnear, I. S., "Cooling Performance Evaluation of Turbine Blades and Nozzle Guide Vanes by Scaled Testing at Other Than Engine Conditions," Scaling For Performance Prediction in Rotodynamic Machines, I Mech E Conference Publications 1977-7, Institution of Mechanical Engineers, London, 1977, Paper C179/77, pp. 49-62.

5 Gladden, H. J.: Extension of Similarity Test Procedures to Cooled Engine Components with Insulating Ceramic Coatings. NASA TP-1615, 1980.

6 Calvert, H. F., et al., "Turbine Cooling Research Facility," NASA TM X-1927, 1970.

7 Stecura, S. and Liebert, C. H., "Thermal Barrier Coating System," U.S. Patent 4,055,705, Oct. 1977.

8 Crowl, R. J. and Gladden, H. J., "Methods and Procedures for Evaluating, Forming, and Installing Small-Diameter Sheathed Thermocouple Wire and Sheathed Thermocouples," NASA TM X-2377, 1971.

9 Gladden, H. J., Gauntner, D. J., and Livingood, J. N. B., "Analysis of Heat-Transfer Tests of an Impingement-Convection-and Film-Cooled Vane in a Cascade," NASA TM X-2376, 1971.

10 Poferl, D. J., Svehla, R. A., and Lewandowski, K., "Thermodynamic and Transport Properties of Air and The Combustion Products of Natural Gas and ASTM A-1 Fuel With Air," NASA TN D-5452, 1969.

11 High Temperature High Strength Nickel Base Alloys, The International Nickel Co., Inc., New York, 1964.

12 Liebert, C. H. and Stepka, F. S., "Industry Tests of NASA Ceramic Thermal Barrier Coating," NASA TP 1425, 1979.

TABLE I. - THERMOCOUPLE LOCATIONS AND COATING THICKNESS

Thermocouple	Distance from leading edge, cm	Dimensionless distance	Ceramic coating thickness,* cm
Suction surface, L = 7.42 cm			Vane 2
1	6.42	0.866	0.033
2	5.07	.684	.030
3	3.88	.523	.028
4	2.60	.351	.041
5	1.32	.178	.030
6	.50	.067	.023
7	0	0	.025
Pressure surface, L = 6.45 cm			
8	0.39	0.061	0.013
9	1.25	.194	.023
10	2.52	.391	.018
11	3.78	.586	.015
12	4.85	.752	-----

*Tolerance ±0.002 cm

TABLE II. - TEST AND ENGINE CONDITIONS

	Test conditions			Engine conditions		
Test vane coating	Gas temperature, K	Gas pressure, atm	Coolant temperature, K	Gas temperature, K	Gas pressure, atm	Coolant temperature, K
None	890	4.5	300	1550	8.3	300
ZrO_2	920	5.2	300	1440	8.6	300

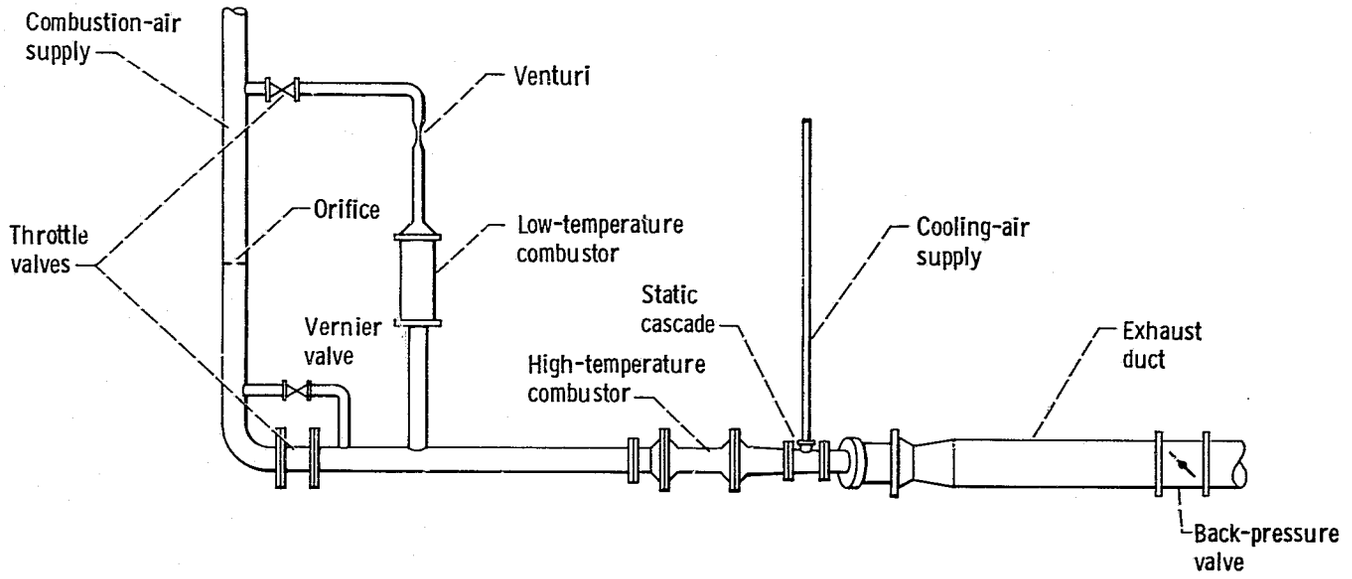

(a) Overall view of facility.

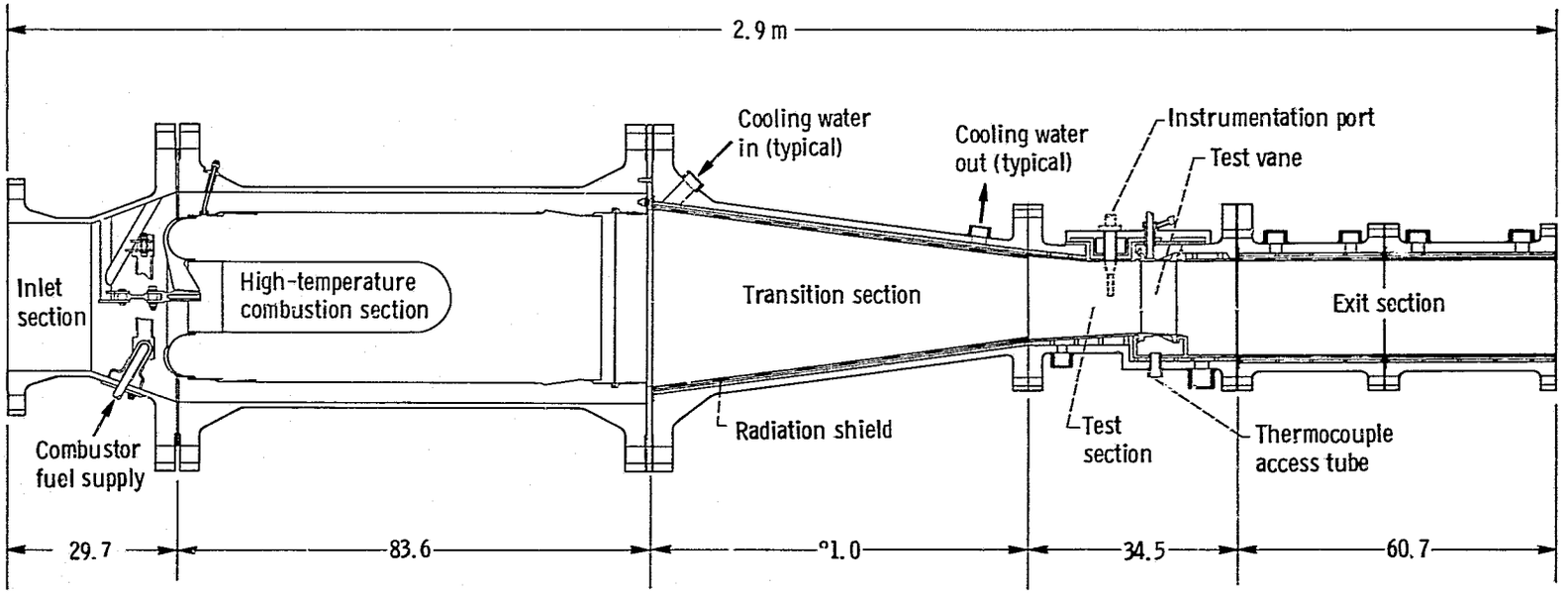

(b) Cross-sectional view of main high-temperature components. (Dimensions are in cm unless noted.)

Figure 1. - Schematic of cascade facility.

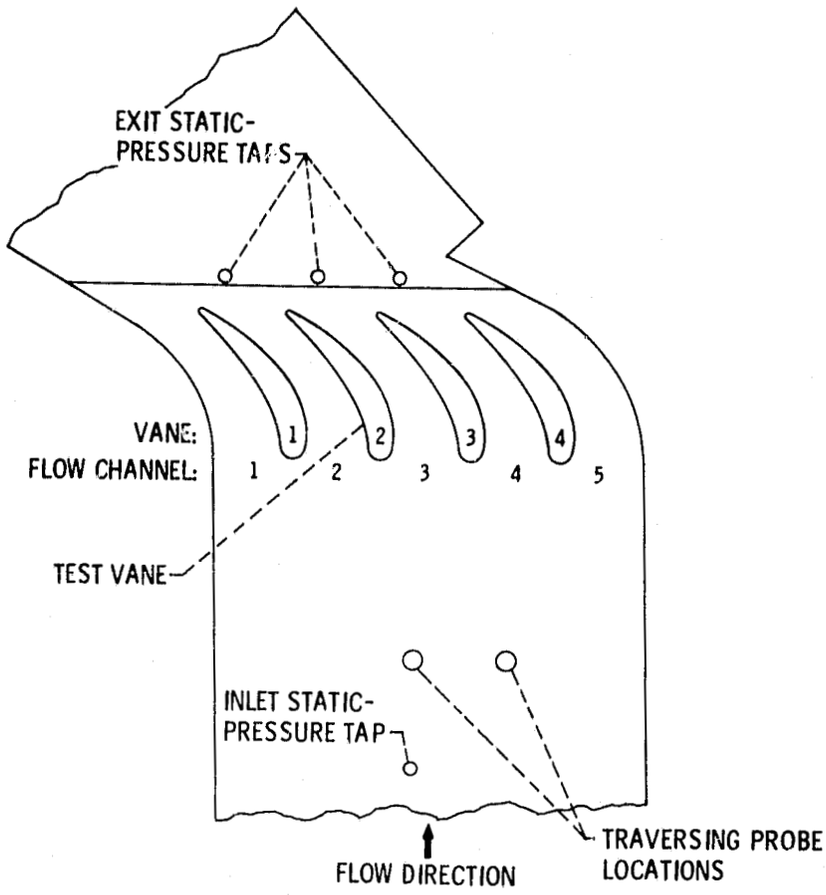

Figure 2. - Vane row and location of instrumentation stations in static cascade test section.

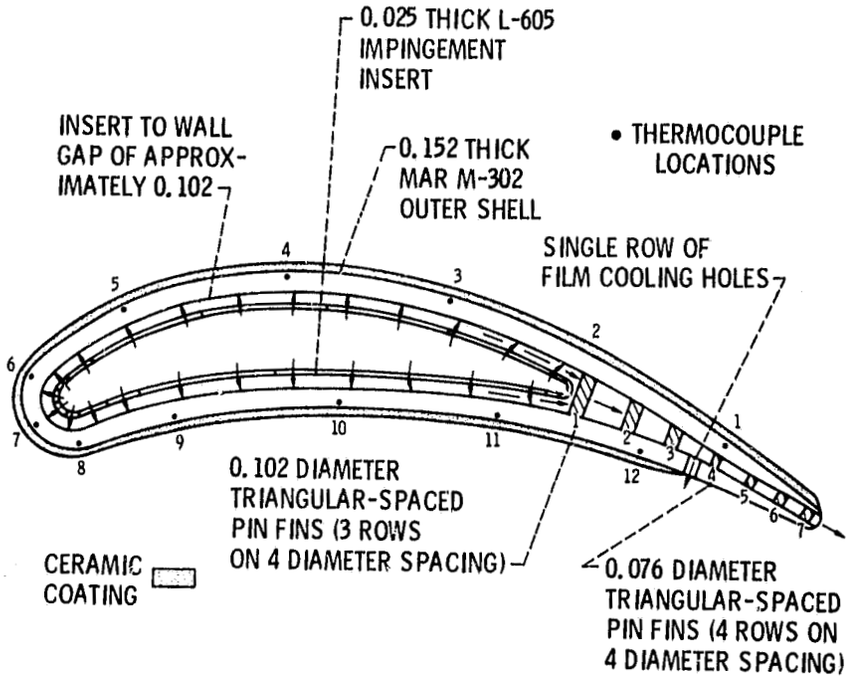

Figure 3. - Schematic cross-sectional midspan view of test vane, showing the internal cooling configuration and the thermocouple locations.

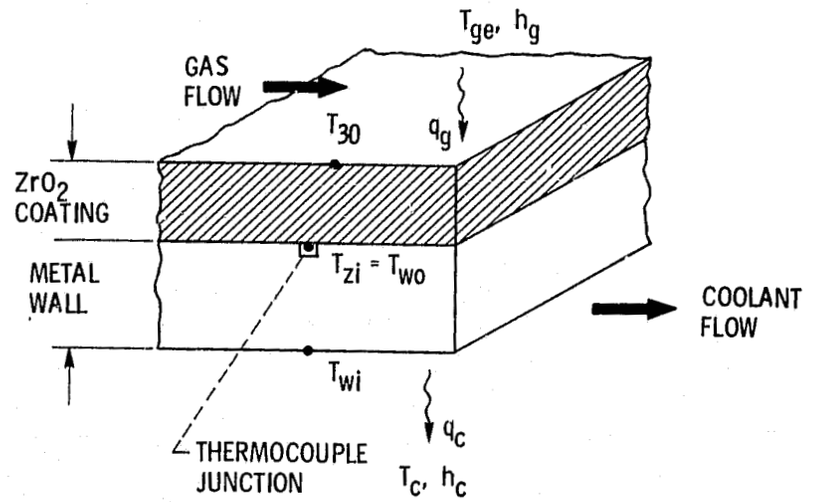

Figure 4. - One-dimensional heat transfer model of airfoil wall with ceramic coating. Thermocouple junction assume to be at the metal-ceramic interface.

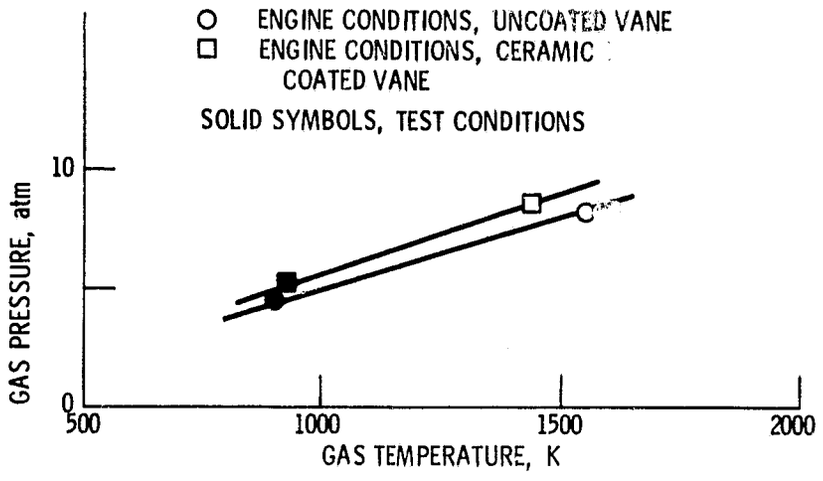

Figure 5. - Similarity relationships for the test and engine conditions investigated.

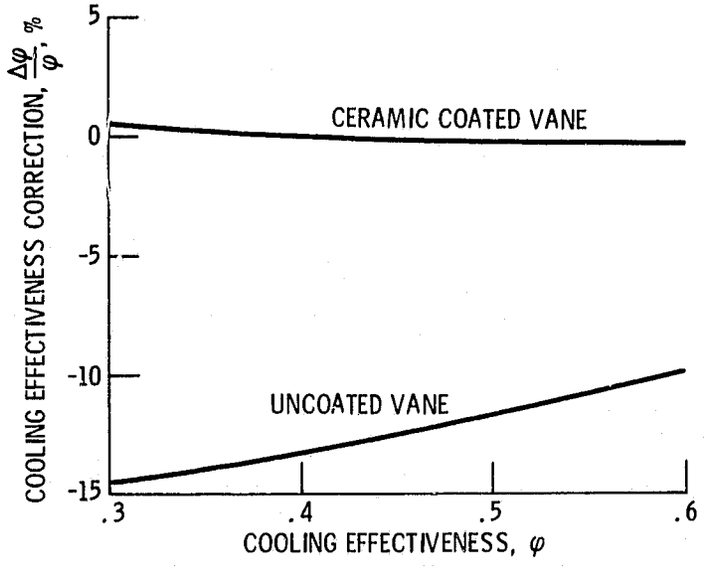

Figure 6. - Test data correction factors for ceramic coated and uncoated vanes.

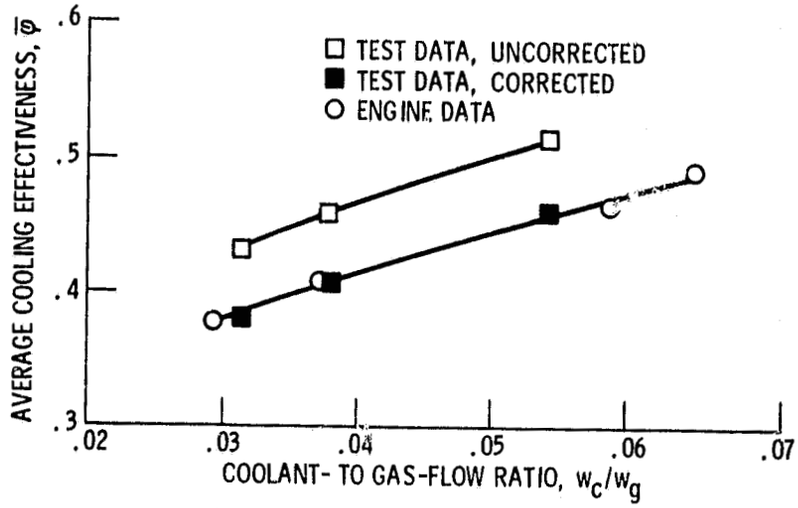

Figure 7. - Average cooling effectiveness test and engine data for an uncoated turbine vane.

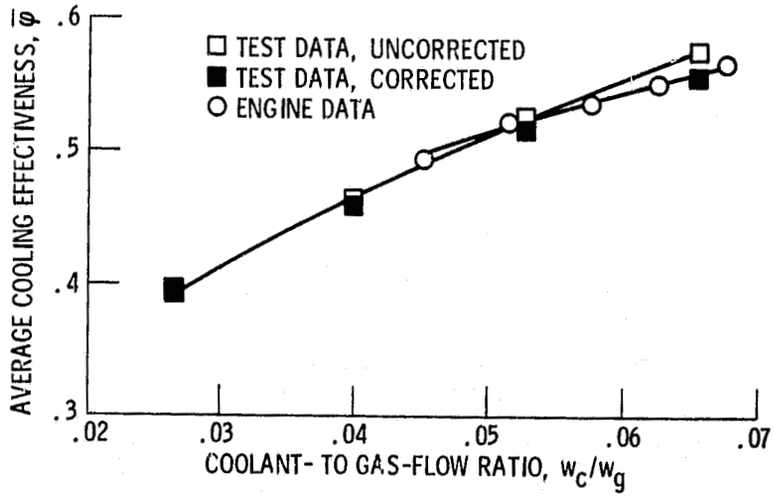

Figure 8. - Average cooling effectiveness test and engine data for a ceramic coated turbine vane.

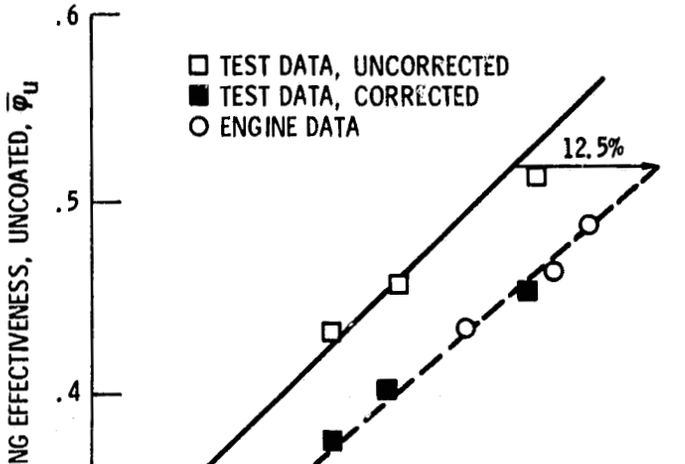

Figure 9. - Comparison of test and engine cooling effectiveness data of ceramic coated and uncoated turbine vanes.